Temperature response of wheat affects final height and the timing of stem elongation under field conditions

Lukas Kronenberg[a], Steven Yates[b], Martin P. Boer[c], Norbert Kirchgessner[a], Achim Walter[a], Andreas Hund[a]

[a] Crop Science, Institute of Agricultural Sciences , ETH Zürich, 8092 Zurich, Switzerland
[b] Molecular Plant Breeding, Institute of Agricultural Sciences , ETH Zürich, 8092 Zurich, Switzerland
[c] Biometris, Wageningen University & Research, 6708 PB Wageningen, The Netherlands

Highlight

We measured ambient temperature response of stem elongation in wheat grown under field conditions. The results indicate that temperature response is highly heritable and linked to the flowering pathway.

Abstract

In wheat, temperature affects the timing and intensity of stem elongation (SE). Genetic variation for this process is therefore important for adaptation. This study investigates the genetic response to temperature fluctuations during SE and its relationship to phenology and height. Canopy height of 315 wheat genotypes (GABI wheat panel) was scanned twice weekly in the field phenotyping platform (FIP) of ETH Zurich using a LIDAR. Temperature response was modelled using linear regressions between SE and mean temperature in each measurement interval. This led to a temperature-responsive (slope) and a temperature-irresponsive (intercept) component.

The temperature response was highly heritable (H^2 = 0.81) and positively related to a later start and end of SE as well as final height. Genome-wide association mapping revealed three temperature-responsive and four temperature-irresponsive quantitative trait loci (QTL). Furthermore, putative candidate genes for temperature-response QTL were frequently related to the flowering pathway in *A. thaliana,* whereas temperature–irresponsive QTLs corresponded with growth and reduced height genes. In combination with *Rht* and *Ppd* alleles, these loci, together with the loci for the timing of SE accounted for 71% of the variability in height.

This demonstrates how high-throughput field phenotyping combined with environmental covariates can contribute to a smarter selection of climate-resilient crops.

Key Words: development, field phenotyping, GWAS, LIDAR, physiology, plant height, temperature response, wheat

Introduction

Temperature is a major abiotic factor affecting plant growth and development. As a consequence of global warming, wheat production could decrease by 6% per °C global

temperature increase (Asseng *et al.*, 2015). While heat stress during critical stages can drastically reduce yield (Gibson and Paulsen, 1999; Farooq *et al.*, 2011), warm temperatures can decrease yield by accelerating development and thereby shortening critical periods for yield formation (Fischer, 1985; Slafer and Rawson, 1994). Despite the clear effect of temperature on growth and phenology, little is known about the genotype-specific response pattern to varying temperature conditions during crop development and its genetic control. We therefore aimed to quantify the genotype-specific temperature-responsiveness of European winter wheat during the stem elongation phase.

Stem elongation (SE) is a critical phase for yield formation in wheat. It occurs between the phenological stages of terminal spikelet initiation and anthesis (Slafer *et al.*, 2015). The start of SE coincides with the transition from vegetative to reproductive development, when the apex meristem differentiates from producing leaf primordia to producing spikelet primordia (Trevaskis *et al.*, 2007; Kamran *et al.*, 2014). During SE, florets are initiated at the spikelets until booting (Kirby, 1988; Slafer *et al.*, 2015). An increased duration of SE increases the number of fertile florets due to longer spike growth and higher dry matter partitioning to the spike (González *et al.*, 2003). This in turn increases the number of grains per spike and therefore yield (Fischer, 1985). Modifying the timing of the critical phenological stages (transition to early reproductive phase and flowering), and thus SE duration, has been proposed as a way to increase wheat yield (Slafer *et al.*, 1996; Miralles and Slafer, 2007; Whitechurch *et al.*, 2007) or at least to mitigate adverse climate change effects on yield e.g. by enhancing earliness to escape heat during flowering (Chapman *et al.*, 2012; Hernandez-Ochoa *et al.*, 2019). The recent warming trend causes a faster advancement in phenology. For example flowering time occurred earlier in Germany throughout the past decade, which is attributable to both, increased temperature and selection for early flowering (Rezaei *et al.*, 2018).

Final height is also an important yield determinant. During the “green revolution” wheat yields increased by the introduction of reduced height genes (*Rht*). The resulting dwarf and semi dwarf varieties benefit from improved resource allocation from the stem to the spike and reduced lodging, allowing more intensive nitrogen application (Hedden, 2003). Gibberellin insensitive *Rht* genes (*Rht-A1*, *Rht-B1*, and *Rht-D1*) were shown to limit cell wall extensibility which decreases growth rates (Keyes *et al.*, 1989) without affecting development (Youssefian *et al.*, 1992). Moreover, the allele *Rht-B1c* (Wu *et al.*, 2011) and the GA sensitive *Rht12* dwarfing gene (Chen *et al.*, 2013) delay heading.

The main abiotic factors affecting the timing of floral initiation and flowering are temperature and photoperiod; with temperature affecting both vernalisation and general rate of development (Slafer *et al.*, 2015). These developmental transitions are controlled by major genes involved in the flowering pathway; namely: vernalisation (*Vrn*), photoperiod (*Ppd*) and earliness per se (*Eps*) genes (Slafer *et al.*, 2015). The *Ppd* and *Vrn* genes define photoperiod and vernalisation requirements which jointly enable the transition to generative development and define time to flowering. Whereas *Eps* genes fine tune the timing of floral transition and flowering, after vernalisation and photoperiod requirements are fulfilled (Zikhali and Griffiths, 2015). While vernalisation and photoperiod response are well known, the role of temperature *per se* remains less clear. Temperature affects all developmental phases and warmer ambient

temperatures generally accelerate growth and development in crops (Slafer and Rawson, 1994, 1995*a*,*c*; Atkinson and Porter, 1996; Fischer, 2011; Slafer *et al.*, 2015). But it is unclear, if temperature response governs growth rate and development independently. If so, the question remains, whether there is enough genetic variability in temperature response to be used in a breeding context (Parent and Tardieu, 2012).

Genotypic variation for growth response to temperature was reported for wheat leaf elongation rate (Nagelmüller *et al.*, 2016), as well as for canopy cover growth (Grieder *et al.*, 2015). Kiss et al. (2017) reported significant genotype by temperature interactions in the timing of SE as well as temperature dependent differences in the expression of *Vrn* and *Ppd* genes under controlled conditions. Under field conditions, the response of stem elongation to temperature has not yet been investigated in high temporal resolution.

In recent years, new high throughput phenotyping technologies have enabled monitoring plant height with high accuracy and frequency in the field (Bendig *et al.*, 2013; Friedli *et al.*, 2016; Holman *et al.*, 2016; Aasen and Bareth, 2018; Hund *et al.*, 2019). We have previously demonstrated that the ETH field phenotyping platform (FIP, Kirchgessner *et al.*, 2016) can be used to accurately track the development of canopy height in a large set of wheat genotypes using terrestrial laser scanning (Kronenberg *et al.*, 2017). Considerable genotypic variation was detected for the start and end of SE which correlated positively with final canopy height (Kronenberg *et al.*, 2017).

While many temperature-independent factors affecting plant height are known, the influences of temperature-dependent elongation and timing of the elongation phase is less clear. We hypothesise that apart from temperature-independent factors, there is a genotype specific response to ambient temperature which affects growth as well as the timing of developmental stages. To address this, we aimed to dissect the process towards final height into the following components: i) temperature-independent elongation, ii) temperature-dependent elongation and iii) the duration of the elongation phase determined by the start and end of the process. To achieve this we present a method to assess and measure these three processes under field conditions by means of high-frequency, high-throughput phenotyping of canopy height development. The resulting data were combined with genetic markers to identify quantitative trait loci controlling the aforementioned processes.

Material and Methods

Experimental setup, phenotyping procedures and extracted traits

Field experiments were conducted in the field phenotyping platform FIP at the ETH research station in Lindau-Eschikon, Switzerland (47.449°N, 8.682°E, 520 m a.s.l.; soil type: eutric cambisol). We used a set of approximately 330 winter wheat genotypes (335 – 352 depending on the experiment) comprising current European elite cultivars (GABI Wheat; Kollers *et al.*, 2013), supplemented with thirty Swiss varieties. These were monitored over three growing seasons in 2015, 2016 and 2017. Briefly, the field experiments were conducted in an augmented design with two replications per genotype using micro plots with a size of 1.4 by 1.1 m. In the growing season 2017, the experiment was repeated again, with minor changes

in genotypic composition. This resulted in 328 genotypes present across all three experiments. Details about the experimental setup for the growing seasons 2015 and 2016 are described in Kronenberg et al. (2017).

Canopy height was measured twice weekly from the beginning of shooting (BBCH 31) using a light detection and ranging (LIDAR) scanner (FARO R Focus3D S 120; Faro Technologies Inc., Lake Mary USA) mounted on the FIP (Kirchgessner *et al.*, 2016). Height measurements were concluded when no further height increase was observed in any of the genotypes. Canopy height data was extracted from the LIDAR data as described in Kronenberg et al. (2017).

The start, end, and duration of SE as well as final canopy height (FH) were extracted from the height data following Kronenberg et al. (2017): FH was defined as the point, after which no increase in height was observed in several consecutive measurements. Normalized canopy height was calculated as percent of FH at each day of measurement for every plot and then linearly interpolated between measurement points. Growing degree-days after sowing until 15% FH (GDD_{15}) and 95% FH (GDD_{95}) were used as proxy traits for start and end of SE, respectively. SE duration was recorded in thermal time (GDD_{SE}) as well as in calendar days ($time_{SE}$), as the difference between GDD_{95} and GDD_{15} (Kronenberg *et al.*, 2017). Heading date was recorded as GDD ($heading_{GDD}$) when 50% of the spikes were fully emerged from the flag leaf sheath (BBCH 59; Lancashire *et al.*, 1991). Heading data for 2015 could not be evaluated due to insufficient data availability. Therefore, a third year of heading data was gathered in 2018, when the experiment was repeated again as described in Anderegg et al., (2020).

In order to investigate short-term growth response to temperature, average daily stem elongation rates (SER) were calculated for each plot as the difference (Δ) in canopy height (CH) between consecultive time points (t):

$$SER = \frac{\Delta CH}{\Delta t} \quad \text{eq. 1}$$

Extracting growth response to temperature

Temperature response was modelled by regressing average daily SER against average temperature of the respective interval for each plot within the respective year following

$$SER = (a \times T) + b_{T_{crit}} + \varepsilon \qquad \text{eq. 2}$$

where *T* is the ambient temperature, *a* is the coefficient of the linear regression (*i.e.* growth response to ambient temperature; $slp_{SER\sim T}$) and *ε* denotes the residual error. b_{Tcrit} is the model intercept at the temperature, at which the correlation between intercept ($int_{SER\sim T}$) and slope is zero (*see below*). Per definition, the intercept of a linear model would be calculated at T = 0 °C, *i.e.* far outside the range of observed temperatures. In the observed data, the intercept at T = 0°C correlated strongly negative with the slope (Fig. 1A) and thus, did not add much additional information concerning the performance of the evaluated genotypes. Likewise, an intercept at 20°C, at the upper range of the observed data correlated strongly positive with the slope (Fig 1A). Grieder *et al*. (2015) performed a similar analysis for the canopy cover development during winter and found a similar, strongly negative correlation between temperature response (slope) and growth at 0°C (intercept). We sequentially calculated the intercept at 0.01°C increments between 1°C and 22°C for each plot within a year.

Subsequently, we calculated the Pearson correlation coefficient between the common slope of these models and each of the different intercepts (Fig 1A). Based on this sequence, we empirically determined the critical temperature value (T_{crit}) at which the correlation between slope and intercept was zero (Fig 1A). Hence, T_{crit} is defined as the temperature at which intercept and slope are independent. Due to this independence, the value of the intercept at T_{crit} can be interpreted as intrinsic growth component independent of temperature response herein referred to as "vigour". Following this, two genotypes can show the same vigour but differ markedly in temperature response (Fig. 1B), have the same temperature response but differ in vigour (Fig. 1C), or differ for both, temperature response and vigour (Fig. 1D).

Statistical Analysis

The data were processed stepwise as follows: i) correction for design factors and spatial trends, ii) application of linear models to each plot to determine growth-response to temperature and iii) prediction of adjusted means and calculation of the heritability for all traits across years.

The spatial correction of canopy height per measurement time point was done using the R-package SpATS (Rodríguez-Álvarez *et al.*, 2018) following

$$Y_{i,j,k} = f(r,c) + G_i + R_j + C_k \qquad \text{eq. 3}$$

where Y is the phenotypic value for the a plot in the jth row in the kth column planted with the ith genotype, $f(r,c)$ is a smoothed bivariate surface defined over rows and ranges of a virtual grid, G_i is the effect of the ith genotype (i = 1, …, n; n= 335 – 352 depending on the year), R_j is the effect of the jth row in the virtual grid and C_k is the effect of the kth range. With the number of genotypes, the number of ranges/rows varied across years (17/21 in 2015, 18/20 in 2016 and 18/21 in 2017, respectively). The replications were arranged diagonally in this grid with a gap of five rows and ranges between them. Thus, e.g. in 2017, replication 1 was at rows 1-21 and ranges 1-18; replication 2 was at rows 24-41 and ranges 27-47 of the virtual grid.

The function $f(r,c)$ describing the bivariate surface can be decompose in a nested-type ANOVA structure as describe by Rodríguez-Álvarez et al. (2018). The number of spline points was set to 2/3 of the total number of rows and ranges in the virtual grid, respectively.

From this model the predicted genotypic best linear unbiased estimates (BLUEs) plus residual error were kept as spatially corrected plot value. Thus, these new plot values were corrected for spatial effect as well as for the random row and range effects and used for the subsequent dynamic model. For a visualisation of the applied SpATS correction, see Fig. S1.

Genotypic BLUEs across the three seasons were calculated for all traits using the R-package asreml-4 (Butler, 2018) following

$$y_{pij} = \mu + G_i + Y_j + GY_{ij} + \varepsilon_{pij} \qquad \text{eq. 4}$$

where y_{pij} is the spatialy corrected plot value of the respective trait (FH, GDD_{15}, GDD_{95}, GDD_{SE}, $time_{SE}$, $int_{SER\sim T}$ or $slp_{SER\sim T}$), μ is the overall mean, G_i the fixed effect of the genotypes common in all three years (i = 1,..,328), Y_j is the fixed effect of the year (j = 2015,…,2017), G_iY_j ist the random genotype-by-year interaction and ε_{pij} is the residual error.

198 In order to estimate best linear unbiased predictors and heritability (H^2) across years, G_i in eq.
199 3 was set as random term and heritability was calculated following (Falconer and Mackay,
200 1996) using

201 $$H^2 = \frac{\sigma_G^2}{\sigma_G^2 + \frac{\sigma_{GY}^2}{3} + \frac{\sigma_\varepsilon^2}{6}} \qquad \text{eq. 5}$$

202 where H^2 is the broad sense heritability, σ_G^2 is the genotypic variance, σ_{GY}^2 is the genotype-by-
203 year interaction variance and σ_ε^2 is the residual variance. For heading data, only one replicate
204 per year was available. Plot corrected values were extracted using SpATS (Rodríguez-Álvarez
205 *et al.*, 2018) and heritability across three years was calculated by omitting the *GY* term in eq.
206 4 and dividing the residual variance by three, based on the three available year-site
207 replications.

208 Genotypic BLUEs across three years were used for subsequent correlation analysis and
209 genome wide association study (GWAS). All statistical analyses were performed in the R
210 environment (R Core Team, 2015).In order to investigate the relationship between FH,
211 temperature response and vigour and to test for confounding *Rht* or *Ppd* effects on
212 temperature response, FH was modelled using the linear model

213 $$y_i = \mu + \sum_{k=1}^{6} \beta_k x_{k,i} + \sum_{k=1}^{5} \sum_{m=k+1}^{6} \beta_{k,m} x_{k,i}\, x_{m,i} + \varepsilon_i \qquad \text{eq. 6}$$

214 where y_i is FH of the ith genotype, μ is the model intercept, β_{1-6} are the main effect estimates
215 of x = $slp_{SER\sim T}$, $int_{SER\sim T}$, GDD_{SE}, *Rht-B1*, *Rht-D1* or *Ppd-D1*, respectively. $\beta_{1,2} - \beta_{5,6}$ are all two-
216 way interaction effects (n = 15) and ε_i is the residual error. Genotypic data for *Rht-B1*, *Rht-D1*
217 and *Ppd-D1* alleles was available for 301 genotypes obtained from Kollers et al. (2014). There,
218 genotyping of the *Rht-1* alleles was performed using pcr markers (Ellis *et al.*, 2002), while *Ppd-*
219 *D1* alleles were genotyped by presence or absence of a 2-kb insertion using specific primers
220 (Beales *et al.*, 2007; Kollers *et al.*, 2014)

221 **Association study**

222 GWAS was performed on the different traits to compare the phenotypic correlations with the
223 underlying genetic architecture of the traits. As a positive control FH data made in Germany
224 and France by Zanke et al., (2014*b*) was also compared and analysed.

225 Genotyping data was made previously by the GABI wheat consortium represented by the
226 Leibniz Institute of Plant Genetics and Crop Plant Research (IPK; Zanke *et al.*, 2014*a*) using the
227 90K illumina SNP-chip (Cavanagh *et al.*, 2013; Wang *et al.*, 2014). Monomorphic SNPs were
228 discarded. The remaining markers were mapped to the IWGSC reference genome (Consortium
229 (IWGSC) *et al.*, 2018) by BLASTN search using an E-value threshold < $1e^{-30}$. The genome
230 position with the lowest E-value was assigned as the respective marker location. Markers that
231 could not be unequivocally positioned were dropped. After filtering SNPs with a minor allele
232 frequency and missing genotype rate < 0.05, a total of 13,450 SNP markers and 315 genotypes
233 remained in the set. The reference genome position of *Rht*, *Ppd*, *Vrn* and putative *Eps* genes

234 was determined with BLASTN search as described above using published GenBank sequences
235 (Table S1).

236 To mitigate against multiple testing, relatedness and population structure; three different
237 methods were used to calculate marker trait associations (MTA) between phenotypic BLUPs
238 and SNP markers:

239 i) We used a mixed linear model (MLM) including principal components among marker
240 alleles as fixed effects and kinship as random effect to account for population
241 structure (Zhang *et al.*, 2010). This approach was chosen to stringently prevent type I
242 errors. The MLM GWAS was performed using the R Package GAPIT (v.2, Tang *et al.*,
243 2016). Kinship was estimated according to VanRaden (2008).
244 ii) In a generalised linear model (GLM) framework implemented in PLINK (Purcell *et al.*,
245 2007), association analysis was performed using SNP haplotype blocks consisting of
246 adjacent SNP triplets. Using haplotype blocks takes the surrounding region of a given
247 SNP into account, thus increasing the power to detect rare variants (Purcell *et al.*,
248 2007)
249 iii) Finally, the FarmCPU method (Liu *et al.*, 2016) was used, which is also implemented in
250 GAPIT. FarmCPU tests individual markers with multiple associated markers as
251 covariates in a fixed effect model. Associated markers are iteratively used in a random
252 effect model to estimate kinship. Confounding between testing markers and kinship
253 is thus removed while controlling type I error, leading to increased power (Liu *et al.*,
254 2016).

255 For all methods, a Bonferroni correction was applied to the pointwise significance threshold
256 of $\alpha = 0.05$, to avoid false-positives. Hence, only markers above $-\log_{10}(P\text{-value}) >= 5.43$
257 considered significant.

258 Linkage disequilibrium (LD) among markers was estimated using the squared correlation
259 coefficient (r^2) calculated with the R package SNPrelate (Zheng *et al.*, 2012). A threshold of r^2
260 $= 0.2$ (Gaut and Long, 2003) was applied to calculate the chromosome specific distance
261 threshold of LD decay. Putative candidate genes were identified by searching the IWGSC
262 annotation of the reference genome (Consortium (IWGSC) *et al.*, 2018) for genes associated
263 with growth and development within the LD distance threshold around the respective MTA.

264 Results

265 **Phenotypic results**

266 We measured the canopy height of 710 – 756 plots per year, containing 335 – 352 wheat
267 genotypes, for three consecutive years. In each season, measurements were made between
268 17 and 22 times during SE. Plot based growth rates within single years extracted from these
269 data indicate a clear relation between growth and temperature for the period of SE, as
270 depicted in Fig. 2. Towards the end of the measurement period in June, there was a larger
271 deviation, which was also reflected in the quality of plot based linear model fits of SER versus
272 temperature (*see* eq. 2), summarized in Fig. S2. For the 2015 and especially the 2016
273 experiment, R^2 values were low and except for the 2017 experiment, the parameter estimates

were not statistically significant (Fig. S2A). Inspection of the best and worst model fits however shows, that failure of fitting the model for single plots was levelled out by the replications within genotypes (Fig. S2B). The weak model fits did therefore not affect the genotype ranking of adjusted means across replications. Analysis of variance revealed significant ($P < 0.001$) genotypic effects for both $slp_{SER\sim T}$ and $int_{SER\sim T}$ across three years. Both traits showed high heritabilities across years ($H^2 = 0.81$ for $slp_{SER\sim T}$ and $H^2 = 0.77$ for $int_{SER\sim T}$; Table 1). Using the BLUEs of $slp_{SER\sim T}$, $int_{SER\sim T}$ and temperature sum for SE (GDD_{SE}), FH could be predicted with high accuracy across different years ($0.85 <= R^2 <= 0.89$) by training a linear model on the BLUEs of one year and predicting it on the BLUEs of another independent year. In order to account for possible confounding *Rht* and *Ppd* effects, the allelic status of *Rht-B1*, *Rht-D1* and *Ppd-D1* were included as contrasts in the model (Table 2). Of the 301 genotypes with available data 7 % and 58 % carried the dwarfing alleles *Rht-B1b* and *Rht-D1b*, respectively, and 13 % carried the photoperiod insensitive allele *Ppd-D1a*. Training the model on the 3-year BLUEs resulted in a prediction accuracy of single years between $R^2 = 0.94$ and $R^2 = 0.95$ (Fig. 3). Type II ANOVA revealed significant effects for $slp_{SER\sim T}$, $int_{SER\sim T}$, GDD_{SE}, *Rht-B1* and *Rht-D1*. A significant ($P < 0.05$) interaction effect was found between *Rht-D1* and *Ppd-D1*. Furthermore, weak interactions ($P < 0.1$) were found for *Rht-B1:Ppd-D1*, $int_{SER\sim T}$*:Rht-B1* and $int_{SER\sim T}$*:Rht-D1* (Table 2). High heritabilities across three years ($0.54 <= H^2 <= 0.98$; Table 1), were also found for the other traits; FH, start of SE, end of SE, SE duration and heading. All traits showed moderate genotype by year interaction effects which were smaller (except for SE duration) than the genotypic effects across years (Table 1).

Phenology, temperature response and final height were positively correlated

To evaluate the relationships between the traits measured, Pearson correlation coefficients were calculated for each trait pair. If not indicated otherwise, the reported correlations were highly significant ($P < 0.001$)

Positive correlations were found among GDD_{15}, GDD_{95} and FH ($0.36 <= r <= 0.64$, Fig. 4), indicating that taller genotypes were generally later in their development towards FH. Temperature response ($slp_{SER\sim T}$) and vigour ($int_{SER\sim T}$) also showed a strong, positive relationship with FH ($r = 0.85$ and $r = 0.65$, respectively). However, only temperature response correlated with GDD_{15} and GDD_{95} ($r = 0.63$ and $r = 59$, respectively), whereas vigour did not ($r < 0.26$, Fig. S3).

As expected, SE duration in thermal time (GDD_{SE}) was negatively correlated with GDD_{15} ($r = -0.44$) and positively correlated with GDD_{95} ($r = 0.4$). But, GDD_{SE} did not correlate with FH ($r = -0.01$, $P = 0.874$) or temperature response ($r = 0.006$, $P = 0.285$), although GDD_{SE} negatively correlated with vigour ($r = -0.32$). In contrast, SE duration in calendar days ($time_{SE}$) was negatively correlated with temperature response ($r = -0.35$) and GDD_{15} ($r = -0.82$), indicating a longer SE phase for earlier genotypes. Heading showed strong positive correlations with GDD_{15} ($r = 0.61$) and GDD_{95} ($r = 0.71$) and a weak correlation to temperature response ($r = 0.29$). Furthermore, heading correlated negatively with $int_{SER\sim T}$ ($r = -0.41$) and showed no correlation to FH ($r = 0$, $P = 0.934$). Other weak correlations ($r < 0.3$), that are not discussed, are shown in Fig. S3.

Linkage disequilibrium and population structure

316 Prior to MTA analysis we evaluated population structure and LD. Principal component analysis
317 of the marker genotypes revealed no distinct substructure in the investigated population. The
318 biplot of the first two principal components showed no apparent clusters, with the first
319 component explaining 8% and the second component explaining 3.3% of the variation in the
320 population (Fig. S4). This is consistent with prior work using the same population (Kollers *et*
321 *al.*, 2013; Yates *et al.*, 2019). On average across all chromosomes, LD decayed below an r^2 of
322 0.2 at a distance of 9 MB. There was however considerable variation in this threshold among
323 the single chromosomes (Table S2).

324 **Association study**

325 Genome-wide association results differed markedly depending on the applied model. Using a
326 MLM with kinship matrix and PCA as covariates resulted in no significant MTA for any trait
327 (Fig. S5). In contrast, the GLM using the haplotype method on temperature response yielded
328 2958 significant MTA for $\alpha < 0.05$ and 1852 MTA for $\alpha < 0.001$ respectively (Fig. S6). However,
329 investigation of the respective QQ-plots showed large *P*-value inflation in the haplotype
330 method whereas the *P*-values were slightly deflated when using the MLM approach (Fig. S5,
331 Fig. S6). In contrast, with FamCPU the QQ-plots (Fig 5) showed no *P*-value inflation, except for
332 some markers. This pattern is expected, if population structure is appropriately controlled.
333 Therefore, FarmCPU was chosen to be the most appropriate method for the given data,
334 despite identifying less significant MTA.

335 As a positive control we compared our FH data and associated markers with data made by
336 Zanke et al (2014*b*) who used the same population and SNP chip in field experiments in France
337 and Germany. Final canopy height correlated strongly between the two studies (r = 0.95),
338 which is in accordance with the high heritability of the trait. In this study, we found ten
339 significant MTA for FH (Table 3, Fig. 5). Zanke et al. (2014*b*) reported 280 significant MTA for
340 FH across several environments. Of these, only marker RAC875_rep_c105718_585 on
341 chromosome 4D overlapped with the MTA found in this study. However, by considering
342 flanking markers, we found that of the remaining nine significant MTA for FH, four were in LD
343 with MTA found by Zanke et al. (2014*b*; Table S3). The significant MTA found for FH in this
344 study are near known genes controlling FH. For example, Tdurum_contig64772_417, is 4 MB
345 upstream of *Rht*-B1 and RAC875_rep_c105718_585, is 7 MB downstream of *Rht*-D1 on their
346 respective group 4 chromosomes.

347 **Temperature-response loci are independent of vigour loci**

348 For $slp_{SER\sim T}$ we detected one significant (LOD = 5.75) MTA on chromosome 1B
349 (wsnp_Ex_c1597_3045682) and two almost significant (LOD = 5.38 / LOD = 5.01) MTA on
350 chromosomes 4B (CAP7_c10839_300) and 5D (IAAV7104), respectively (Fig. 5). All associated
351 markers for $slp_{SER\sim T}$ yielded small but significant allelic effects ranging from -0.061 mm $°C^{-1}d^{-1}$
352 to -0.051 mm $°C^{-1}d^{-1}$ (Table 3). The GWAS for $int_{SER\sim T}$ yielded four significant MTA on
353 chromosomes 2B, 4B, 4D and 5D respectively (Table 3, Fig. 5). Start and end of SE yielded four
354 MTA each and heading yielded eight MTA (Table 3, Fig. 5).

355 Comparing the GWAS results for temperature response, vigour, FH, GDD_{15}, GDD_{95} and heading
356 revealed no common quantitative trait loci (QTL) between $slp_{SER\sim T}$ and any other trait. Only

357 one marker (Excalibur_c74858_243) was significantly associated with both GDD_{15} and GDD_{95},
358 as well as heading. The lack of overlap, of MTA, between temperature response, vigour and
359 timing of critical stages indicate they are genetically independent. However, there is a genetic
360 connection between vigour and FH on the one hand and between the start and end of SE and
361 heading on the other.

362 To identify potential causative genes underlying the QTL, we searched the reference genome
363 annotation around the respective QTL intervals. For temperature response we found an
364 increased presence of genes or gene homologues involved in the flowering pathway, i.e.
365 *EARLY FLOWERING 3*, *FRIGIDA* and *CONSTANS* (Table 4). Around the QTL associated with
366 vigour the annotation showed genes associated with growth (i.e. *GRAS, CLAVATA, BSU1,*
367 *ARGONAUTE*) as well as developmental progress (i.e. *Tesmin/TSO1-like CXC domain, BEL1,*
368 *AGAMOUS* (Table 5). Importantly, we found *GAI-like protein 1* 6MB upstream of marker
369 Kukri_rep_c68594_530, which we identified as *Rht-D1* by blasting the *Rht*-D1 sequence
370 (GeneBank ID AJ242531.1) against the annotated reference genome. Genes putatively
371 underlying the QTL for heading, GDD_{15} and GDD_{95} are listed in the supplementary tables S4 –
372 S6. As expected, genes or gene homologues associated with the flowering pathway were
373 found in the vicinity of the MTA for heading. The common QTL for heading, GDD_{15} and GDD_{95}
374 on chromosome 5B (Excalibur_c74858_243) was found to be 6.6 MB upstream of *FLOWERING*
375 *LOCUS T* (Tables S4-S6). Other flowering associated genes found near the heading QTL were
376 CONSTANS, *FRIGIDA*, and a *FLOWERING LOCUS C* associated protein (Table S4). Moreover, a
377 number of putative response regulators as well as genes putatively involved in light control of
378 development (i.e. FAR1-RELATED SEQUENCE; Lin and Wang, 2004) were found near the
379 heading QTL (Table S4). The remaining QTL for GDD_{95} were near genes associated with
380 developmental progress and flowering, e.g. *AGAMOUS*, *MEI2-like 1*, *HAPPLESS 2* and *BEL1*
381 (Table S5). Genes near the remaining QTL for GDD_{15} were associated with developmental
382 progress (*i.e. FLOWERING LOCUS T, BEL1*, *TERMINAL EAR1-like,* and *FAR1-RELATED*
383 *SEQUENCE*) as well as growth (*i.e. CLAVATA* and DELLA; Table S6).

384 **Vigour, temperature response and the timing of SE affect final height**

385 The phenotypic correlations show a strong connection between temperature response, vigour
386 and FH as well as weaker connections between GDD_{15}, GDD_{95} and FH. In order to examine this
387 interdependency on a genetic level, we used a linear model to predict FH with the SNP alleles
388 of the QTL for $slp_{SER\sim T}$, $int_{SER\sim T}$, GDD_{15} and GDD_{95} as predictors. The model was able to predict
389 FH with an accuracy R^2 = 0.5, however, clusters in the data showed clear effects of *Rht-D1* and
390 *Ppd-D1* alleles (Fig. 6A). Adding *Rht-B1*, *Rht-D1* and *Ppd-D1* alleles as predictors increased the
391 prediction accuracy to R^2 = 0.71 (Fig 6B). There were significant contributions by QTL of all
392 three traits, however, their effect were small compared to the obvious effects of *Rht-B1, Rht-*
393 *D1 and Ppd-D1* (Table 6). Including all two-way interaction effects among the QTL, *Rht-1* and
394 *Ppd-1* increased the prediction accuracy to R^2 = 0.87 (Fig. 6C) indicating a fine-tuning effect of
395 temperature response, vigour and timing of SE towards FH.

Discussion

In this study we present a method to measure temperature response during stem elongation of wheat using high throughput phenotyping of canopy height in the field. We found a genotype-specific response of wheat to change in ambient temperature which was correlated with the timing of the developmental key stages. We decomposed this growth dynamics into a genotype-specific vigour component and temperature response component using regression models. We further related these parameters to plant height and the timing of developmental key stages.

Linear regression models were used to describe wheat growth response to temperature for leaf elongation (Nagelmüller *et al.*, 2016), canopy cover (Grieder *et al.*, 2015) as well as stem elongation rate (Slafer and Rawson, 1995*a*). Others proposed the use of a more complex, Arrhenius type of peak function to account for decreasing growth rates at supra optimal temperatures (Parent and Tardieu, 2012). However such models are mainly applicable when the temperatures experienced by the crop exceed the temperature optimum. Wheat has its temperature-optimum at around 27°C (Parent and Tardieu, 2012). Temperatures in the measured growth intervals during SE did not exceed 25°C and given the temporal resolution of the data, a simple linear model is justified (Parent *et al.*, 2018).

The results of the correlation analysis show a clear connection between FH and temperature response ($slp_{SER\sim T}$) as well as between FH and vigour ($int_{SER\sim T}$). This is consistent with our hypothesis that FH can be described as a function of temperature-independent growth processes and as a function of temperature response during SE. Importantly, among all components, the temperature response was a significant driver of FH and also had a strong influence on the timing. Temperature response delayed the beginning of SE leading to a later start and end of the whole phase. This finding might appear counter intuitive: given the assumption that plants develop faster under higher ambient temperatures a more responsive genotype should develop faster compared to a less responsive one. Slafer and Rawson (1995*b*) reported an accelerated development towards floral transition with increasing temperatures up to 19°C whereas higher temperatures slowed development. In that respect, a more responsive genotype would experience a stronger delay of floral transition under warm temperatures.

In terms of their correlation to FH, the effects of the timing of start and end of SE are less distinct. FH was more a function of faster growth than a longer duration of growth, especially since genotypes with a strong temperature response had a shorter duration of SE. However, the timing of start and end of SE was linked with temperature response. Based on this result and the according correlations, it would appear that temperature response influences FH directly as well as indirectly by mediating start and end of SE. Surprisingly, we found no correlation between heading and FH despite the positive correlation of both traits with GDD_{95}. A correlation between heading date and FH would be therefore expected. Previous studies reporting pleiotropic effects between plant height and heading time (Griffiths *et al.*, 2010; Mo *et al.*, 2018).

436 The question, whether these trait correlations are due to pleiotropic effects will substantially
437 impact the breeding strategy (Chen and Lübberstedt, 2010). If the relationship between
438 phenology, FH and temperature response would be to a large degree pleiotropic, these traits
439 could not be independently selected. Alternative explanations are linkage and population
440 structure. The GABI wheat panel is made of wheat varieties from different regions of Europe.
441 As the examined traits are major drivers of adaptation to the different regions of Europe, we
442 anticipate a very strong selection for both, temperature response as well as timing of critical
443 stages. Even if there is no apparent population structure at neutral markers, there may be a
444 strong population structure at selected loci with strong effect on local adaptation. Our
445 phenotypic results showed a significant interaction effect between *Ppd-D1* and *Rht-D1* on final
446 canopy height, indicating either a co-selection or a pleiotropic effect of *Ppd-D1*. Pleiotropic
447 effects between height and flowering time are known for maize and rice. For example, the
448 *DWARF8* gene of maize encoding a DELLA protein is associated with height and flowering time
449 (Lawit *et al.*, 2010) and strongly associated with climate adaptation (Camus-Kulandaivelu *et*
450 *al.*, 2006, page). The rice *GHD7* locus has a strong effect on number of days to heading, number
451 of grains per panicle, plant height and stem growth (Xue *et al.*, 2008). In wheat, the dwarf
452 gene *Rht-12* was shown to have a delaying effect on heading (Worland *et al.*, 1994; Chen *et*
453 *al.*, 2013) as well as an additive interaction effect with *Ppd-D1* on plant height (Chen *et al.*,
454 2018). Furthermore, it was shown that the tall *Rht-D1a* and the photoperiod sensitive *Ppd-*
455 *D1b* allele positively affect leaf area and spike length throughout SE (Guo *et al.*, 2018). To
456 further examine the relationship among the different traits, we consider the following GWAS
457 analysis using stringent correction of population structure.

458 The GWAS results indicate an independent genetic control of FH, temperature response and
459 the timing of critical stages. Whereas vigour and FH as well as heading time, start and end of
460 SE appear to be partly linked. Yet, FH could be predicted with surprising accuracy using the
461 QTL for temperature response, vigour, start and end of SE which reflects the correlations
462 found in the phenotypic data.

463 Previous studies investigating the control of developmental key stages in wheat with respect
464 to temperature generally adopted the concept, that after fulfilment of photoperiod and
465 vernalisation, *Eps* genes act as fine tuning factors independent of environmental stimuli
466 (Kamran *et al.*, 2014; Zikhali and Griffiths, 2015). Increasing temperature, apart from
467 vernalisation is thought to generally quicken growth and development independent of the
468 cultivar (Slafer and Rawson, 1995*b*; Porter and Gawith, 1999; Slafer *et al.*, 2015). A genotype-
469 specific temperature effect on the duration of different phases was not considered (Takahashi
470 &Yasuda 1971, Slafer & Rawson 1995c). It was however reported, that photoperiod effects
471 vary depending on temperature (Slafer and Rawson, 1995*c*). Under long days, Hemming et al.
472 (2012) reported faster development and fewer fertile florets under high compared to low
473 temperatures. Temperature-dependent effects were also found for different *Eps* QTL (Slafer
474 and Rawson, 1995*c*; Gororo *et al.*, 2001). It has previously been suggested, that *Eps* effects
475 could be associated with interaction effects between genotype and temperature fluctuations
476 (Slafer and Rawson, 1995*c*; van Beem *et al.*, 2005).

477 The mechanisms of ambient temperature sensing and of its effects on growth and
478 development are not yet well understood (Sanchez-Bermejo and Balasubramanian, 2016).

479 However, important findings regarding ambient temperature effects on flowering time as well
480 as on hypocotyl elongation have come from *Arabidopsis thaliana* (Wigge, 2013). With respect
481 to these two traits, Sanchez-Bermejo and Balasubramanian (2016) reported distinct genotypic
482 differences in temperature-sensitivity. According to their results, the flowering pathway genes
483 *FRIGIDA* (*FRI*), *FLOWERING LOCUS C* (*FLC*) and *FLOWERING LOCUS T* (*FT*) are major candidate
484 genes for ambient temperature mediated differences in flowering time (Sanchez-Bermejo and
485 Balasubramanian, 2016). In the present study, we found *FRI* homologues near two of the three
486 QTL for temperature response. *FRI* and *FLC* act as main vernalisation genes in *A. thaliana*
487 (Johanson *et al.*, 2000; Amasino and Michaels, 2010). In wheat, these genes are not yet well
488 described. However, *FLC* orthologues were found to act as flowering repressors regulated by
489 vernalisation in monocots (Sharma *et al.*, 2017).

490 The most promising candidate gene for temperature response found near the QTL on
491 chromosome 1B is *EARLY FLOWERING 3* (*ELF3*). In *Arabidopsis*, *ELF3* was found to be a core
492 part of circadian clock involved in ambient temperature response (Thines and Harmon, 2010).
493 In Barley, *ELF3* was shown to be involved in the control of temperature dependent expression
494 of flowering time genes (Ejaz and von Korff, 2017). A mutant *ELF3* accelerated floral
495 development under high ambient temperatures while maintaining the number of seeds (Ejaz
496 and von Korff, 2017). Furthermore, *ELF3* has been reported as a candidate gene for *Eps1* in
497 Triticum monococcum (Alvarez *et al.*, 2016) as well as in wheat (Zikhali *et al.*, 2016). A recent
498 study in wheat showed an interaction between *Eps-D1* and ambient temperature which
499 corresponded to different expression of *ELF3* (Ochagavía *et al.*, 2019). In this study, we directly
500 measured growth response to temperature during SE and found a significant MTA near *ELF3*
501 on chromosome 1B. Following Ochagavía *et al.* (2019), this indicates that growth response to
502 temperature is connected to *Eps-B1* which is homologue to *Eps-D1*. Furthermore, the reported
503 temperature by *Eps-D1* interaction effects on heading by Ochagavía *et al.* (2019) are in
504 agreement with the correlations found among growth response to temperature, GDD_{15}, GDD_{95}
505 and heading in the present study.

506 One important aspect we could not address in this study is the interaction of genotype specific
507 temperature response with vernalisation and photoperiod (Slafer and Rawson, 1995*c*; Gol *et*
508 *al.*, 2017; Kiss *et al.*, 2017). Due to the climate conditions in Switzerland, we expect fulfilment
509 of vernalisation requirement in all genotypes. However, due to the broad geographic origin of
510 the investigated genotypes, the relationship between temperature response and the timing
511 of SE might be confounded by different photoperiod requirements. Nevertheless, the
512 correlation between earliness and temperature response are in agreement with Ochagavia et
513 al. (2019). It also remains unclear, if and to which extent temperature response varies across
514 different developmental phases and how temperature response relates to other
515 environmental stimuli such as vapour pressure deficit or radiation. Nevertheless, the results
516 of this study present valuable information towards a better understanding of temperature
517 response in wheat and may be of great importance for breeding. Temperature response could
518 provide a breeding avenue for local adaptation as well as the control of plant height.

519 With the recent advancements in UAV-based phenotyping techniques, the growth of canopy
520 cover and canopy height can be measured using image segmentation and structure from
521 motion approaches (Bareth *et al.*, 2016; Aasen and Bareth, 2018; Roth *et al.*, 2018). Thus,

temperature response can be investigated during the vegetative canopy cover development (Grieder *et al.*, 2015) and during the generative height development as demonstrated here. It can also be assessed in indoor platforms (e.g. Parent and Tardieu, 2012) and the field using leaf length tracker (Nagelmüller *et al.*, 2016) measuring short-term responses of leaf growth to diurnal changes in temperature. Combining this information may greatly improve our understanding about the genetic variation in growth response to temperature.

Together, the results of this study indicate that temperature response may be exploitable as a breeding trait to adjust phenology towards specific environments, either through phenotypic or marker assisted selection. Furthermore, a better understanding of temperature response may enhance the capability of crop models to predict crop performance under future climate change scenarios.

Conclusion and outlook

Modern phenotyping platforms hold great promise to map the genetic factors driving the response of developmental processes to environmental stimuli. To the best of our knowledge, this is the first experiment dissecting the SE process into its underlying components: temperature-dependent elongation, temperature-independent vigour and elongation duration. The independent loci detected for these traits suggest, that it is possible to select them independently. The detected loci may be used to fine tune height and the beginning and end of SE as they explain a substantial part of the overall genotypic variation. With increases in automation, growth processes may be monitored in the field on a daily basis or even multiple times per day. This will increase the precision in assessing genotype responses to the fluctuation in meteorological conditions and will allow quantifying the relationship of these responses to yield. Remote sensing by means of unmanned aerial vehicles in combination with photogrammetric algorithms will allow to measure these traits in breeding nurseries. We believe that this is paving the road for a more informed selection to climate adaptation within individual growing seasons.

Supplementary Data

Fig. S1: Correction of canopy height for spatial as well as random row and range effects.

Fig. S2: Summary of plot based linear model fits of stem elongation rate vs. temperature.

Fig. S3: Pearson correlation coefficients among 3-year BLUES of all investigated traits.

Fig. S4: Principal component analysis among marker genotypes.

Fig. S5: Manhattan plots and quantile-quantile plots depicting the GWAS results using the MLM approach.

Fig. S6: Manhattan plots and quantile-quantile plots depicting the GWAS results using the GLM approach.

Table S1: Genes of interest related to floral transition and flowering.

Table S2: Chromosome wise distance thresholds for LD-decay < $r^2 = 0.2$

Table S3: Corresponding marker-trait associations for final canopy height with respect to Zanke et al. 2016.

Table S4: Selected putative candidate genes for $heading_{GDD}$ from the IWGSC reference genome annotation.

Table S5: Selected putative candidate genes for GDD_{95} from the IWGSC reference genome annotation.

Table S6: Selected putative candidate genes for GDD_{15} from the IWGSC reference genome annotation.

Table S7: 3-year BUEs of the investigated traits FH, $heading_{GDD}$, GDD_{15}, GDD_{95}, GDD_{SE}, $time_{SE}$, $slp_{SER\sim T}$, $int_{SER\sim T}$.

Data Availability

Processed phenotypic data is available as supplementary data. Unprocessed data and analysis scripts are available from the authors upon reasonable request.

Acknowledgements

We sincerely thank Hansueli Zellweger for managing and nursing our field experiments. We further thank the members of the ETH crop science and the ETH molecular plant breeding groups, especially Michelle Nay and Beat Keller, for many fruitful discussions. We also thank Martina Binder for doing the correlation analysis between the FH data of this study and the data made by Zanke et al. (2014*b*) in the framework of her MSc-Thesis. We would like to thank Marion Röder (IPK Gatersleben) for supply of the GABI wheat panel including genetic information. Finally, we thank the anonymous reviewers for their helpful comments and suggestions. This work was supported by the Swiss National Foundation (SNF) in the framework of the project PhenoCOOL (project no. 169542).

Author contribution

LK conducted the laser scans, did all statistical analyses and drafted the manuscript; SY assisted with the GWAS and candidate gene evaluation; MB assisted with the spatial correction; NK developed the analysis pipeline for the laser scans; AW drafted the grant application and supervised the overall concept; AH made the experimental design, developed the phenotyping models and assisted with the statistical analysis. All authors contributed to the drafting of the manuscript.

References

Aasen H, Bareth G. 2018. Spectral and 3D Nonspectral Approaches to Crop Trait Estimation Using Ground and UAV Sensing. In: Thenkabail PS, Lyon JG, Huete A, eds. Hyperspectral

Remote Sensing Of Vegetation. Biophysical and Biochemical Characterization and Plant Species Studies. CRC Press, 103–131.

Alvarez MA, Tranquilli G, Lewis S, Kippes N, Dubcovsky J. 2016. Genetic and physical mapping of the earliness per se locus Eps-Am1 in Triticum monococcum identifies EARLY FLOWERING 3 (ELF3) as a candidate gene. Functional & Integrative Genomics **16**, 365–382.

Amasino RM, Michaels SD. 2010. The Timing of Flowering. Plant Physiology **154**, 516–520.

Anderegg J, Yu K, Aasen H, Walter A, Liebisch F, Hund A. 2020. Spectral Vegetation Indices to Track Senescence Dynamics in Diverse Wheat Germplasm. Frontiers in Plant Science **10**.

Asseng S, Ewert F, Martre P, *et al.* 2015. Rising temperatures reduce global wheat production. Nature Climate Change **5**, 143–147.

Atkinson D, Porter JR. 1996. Temperature, plant development and crop yields. Trends in Plant Science **1**, 119–124.

Bareth G, Bendig J, Tilly N, Hoffmeister D, Aasen H, Bolten A. 2016. A Comparison of UAV- and TLS-derived Plant Height for Crop Monitoring: Using Polygon Grids for the Analysis of Crop Surface Models (CSMs). Photogrammetrie - Fernerkundung - Geoinformation **2016**, 85–94.

Beales J, Turner A, Griffiths S, Snape JW, Laurie DA. 2007. A Pseudo-Response Regulator is misexpressed in the photoperiod insensitive Ppd-D1a mutant of wheat (Triticum aestivum L.). Theoretical and Applied Genetics **115**, 721–733.

van Beem J, Mohler V, Lukman R, van Ginkel M, William M, Crossa J, Worland AJ. 2005. Analysis of Genetic Factors Influencing the Developmental Rate of Globally Important CIMMYT Wheat Cultivars. Crop Science **45**, 2113–2119.

Bendig J, Bolten A, Bareth G. 2013. UAV-based Imaging for Multi-Temporal, very high Resolution Crop Surface Models to monitor Crop Growth Variability. PFG Photogrammetrie, Fernerkundung, Geoinformation, 551–562.

Butler D. 2018. *asreml: Fits the Linear Mixed Model*.

Camus-Kulandaivelu L, Veyrieras J-B, Madur D, Combes V, Fourmann M, Barraud S, Dubreuil P, Gouesnard B, Manicacci D, Charcosset A. 2006. Maize Adaptation to Temperate Climate: Relationship Between Population Structure and Polymorphism in the Dwarf8 Gene. Genetics **172**, 2449–2463.

Cavanagh CR, Chao S, Wang S, *et al.* 2013. Genome-wide comparative diversity uncovers multiple targets of selection for improvement in hexaploid wheat landraces and cultivars. Proceedings of the National Academy of Sciences **110**, 8057–8062.

Chapman SC, Chakraborty S, Dreccer MF, Howden SM. 2012. Plant adaptation to climate change—opportunities and priorities in breeding. Crop and Pasture Science **63**, 251–268.

Chen L, Du Y, Lu Q, *et al.* 2018. The Photoperiod-Insensitive Allele Ppd-D1a Promotes Earlier Flowering in Rht12 Dwarf Plants of Bread Wheat. Frontiers in Plant Science **9**.

Chen Y, Lübberstedt T. 2010. Molecular basis of trait correlations. Trends in Plant Science **15**, 454–461.

Chen L, Phillips AL, Condon AG, Parry MAJ, Hu Y-G. 2013. GA-Responsive Dwarfing Gene Rht12 Affects the Developmental and Agronomic Traits in Common Bread Wheat. PLoS ONE **8**.

Consortium (IWGSC) TIWGS, Investigators IR principal, Appels R, *et al.* 2018. Shifting the limits in wheat research and breeding using a fully annotated reference genome. Science **361**, eaar7191.

Ejaz M, von Korff M. 2017. The Genetic Control of Reproductive Development under High Ambient Temperature. Plant Physiology **173**, 294–306.

Ellis M, Spielmeyer W, Gale K, Rebetzke G, Richards R. 2002. 'Perfect' markers for the Rht-B1b and Rht-D1b dwarfing genes in wheat. Theoretical and Applied Genetics **105**, 1038–1042.

Falconer DS, Mackay TFC. 1996. *Introduction to Quantitative Genetics*. Essex, England: Benjamin Cummings.

Farooq M, Bramley H, Palta JA, Siddique KHM. 2011. Heat Stress in Wheat during Reproductive and Grain-Filling Phases. Critical Reviews in Plant Sciences **30**, 491–507.

Fischer RA. 1985. Number of kernels in wheat crops and the influence of solar radiation and temperature. The Journal of Agricultural Science **105**, 447–461.

Fischer RA. 2011. Wheat physiology: a review of recent developments. Crop and Pasture Science **62**, 95–114.

Friedli M, Kirchgessner N, Grieder C, Liebisch F, Mannale M, Walter A. 2016. Terrestrial 3D laser scanning to track the increase in canopy height of both monocot and dicot crop species under field conditions. Plant Methods **12**, 9.

Gaut BS, Long AD. 2003. The Lowdown on Linkage Disequilibrium. The Plant Cell **15**, 1502–1506.

Gibson LR, Paulsen GM. 1999. Yield Components of Wheat Grown under High Temperature Stress during Reproductive Growth. Crop Science **39**, 1841–1846.

Gol L, Tomé F, von Korff M. 2017. Floral transitions in wheat and barley: interactions between photoperiod, abiotic stresses, and nutrient status. Journal of Experimental Botany **68**, 1399–1410.

González FG, Slafer GA, Miralles DJ. 2003. Floret development and spike growth as affected by photoperiod during stem elongation in wheat. Field Crops Research **81**, 29–38.

Gororo NN, Flood RG, Eastwood RF, Eagles HA. 2001. Photoperiod and Vernalization Responses in Triticum turgidum × T. tauschii Synthetic Hexaploid Wheats. Annals of Botany **88**, 947–952.

Grieder C, Hund A, Walter A. 2015. Image based phenotyping during winter: a powerful tool to assess wheat genetic variation in growth response to temperature. Functional Plant Biology **42**, 387–396.

Griffiths S, Simmonds J, Leverington M, Wang Y, Fish L, Sayers L, Alibert L, Orford S, Wingen L, Snape J. 2010. Meta-QTL analysis of the genetic control of crop height in elite European winter wheat germplasm. Molecular Breeding **29**, 159–171.

Guo Z, Liu G, Röder MS, Reif JC, Ganal MW, Schnurbusch T. 2018. Genome-wide association analyses of plant growth traits during the stem elongation phase in wheat. Plant Biotechnology Journal **16**, 2042–2052.

Hedden P. 2003. The genes of the Green Revolution. Trends in Genetics **19**, 5–9.

Hemming MN, Walford SA, Fieg S, Dennis ES, Trevaskis B. 2012. Identification of High-Temperature-Responsive Genes in Cereals. Plant Physiology **158**, 1439–1450.

Hernandez-Ochoa IM, Luz Pequeno DN, Reynolds M, *et al.* 2019. Adapting irrigated and rainfed wheat to climate change in semi-arid environments: Management, breeding options and land use change. European Journal of Agronomy **109**, 125915.

Holman F, Riche A, Michalski A, Castle M, Wooster M, Hawkesford M. 2016. High Throughput Field Phenotyping of Wheat Plant Height and Growth Rate in Field Plot Trials Using UAV Based Remote Sensing. Remote Sensing **8**, 1031.

Hund A, Kronenberg L, Anderegg J, Yu K, Walter A. 2019. Non-invasive field phenotyping of cereal development. In: Ordon F, Friedt W, eds. Advances in breeding techniques for cereal crops. Cambridge UK: Buleigh Dodds Science Publishing.

Johanson U, West J, Lister C, Michaels S, Amasino R, Dean C. 2000. Molecular Analysis of FRIGIDA, a Major Determinant of Natural Variation in Arabidopsis Flowering Time. Science **290**, 344–347.

Kamran A, Iqbal M, Spaner D. 2014. Flowering time in wheat (Triticum aestivum L.): a key factor for global adaptability. Euphytica **197**, 1–26.

Keyes GJ, Paolillo DJ, Sorrells ME. 1989. The Effects of Dwarfing Genes Rht1 and Rht2 on Cellular Dimensions and Rate of Leaf Elongation in Wheat. Annals of Botany **64**, 683–690.

Kirby EJM. 1988. Analysis of leaf, stem and ear growth in wheat from terminal spikelet stage to anthesis. Field Crops Research **18**, 127–140.

Kirchgessner N, Liebisch F, Yu K, Pfeifer J, Friedli M, Hund A, Walter A. 2016. The ETH field phenotyping platform FIP: a cable-suspended multi-sensor system. Functional Plant Biology **44**, 154–168.

Kiss T, Dixon LE, Soltész A, *et al.* 2017. Effects of ambient temperature in association with photoperiod on phenology and on the expressions of major plant developmental genes in wheat (Triticum aestivum L.). Plant, Cell & Environment **40**, 1629–1642.

Kollers S, Rodemann B, Ling J, *et al.* 2013. Whole Genome Association Mapping of Fusarium Head Blight Resistance in European Winter Wheat (Triticum aestivum L.). PLOS ONE **8**, e57500.

Kollers S, Rodemann B, Ling J, *et al.* 2014. Genome-wide association mapping of tan spot resistance (Pyrenophora tritici-repentis) in European winter wheat. Molecular Breeding **34**, 363–371.

Kronenberg L, Yu K, Walter A, Hund A. 2017. Monitoring the dynamics of wheat stem elongation: genotypes differ at critical stages. Euphytica **213**, 157.

Lancashire P, Bleiholder H, Vandenboom T, Langeluddeke P, Stauss R, Weber E, Witzenberger A. 1991. A Uniform Decimal Code for Growth-Stages of Crops and Weeds. Annals of Applied Biology **119**, 561–601.

Lawit SJ, Wych HM, Xu D, Kundu S, Tomes DT. 2010. Maize DELLA Proteins dwarf plant8 and dwarf plant9 as Modulators of Plant Development. Plant and Cell Physiology **51**, 1854–1868.

Lin R, Wang H. 2004. Arabidopsis *FHY3/FAR1* Gene Family and Distinct Roles of Its Members in Light Control of Arabidopsis Development. Plant Physiology **136**, 4010–4022.

Liu X, Huang M, Fan B, Buckler ES, Zhang Z. 2016. Iterative Usage of Fixed and Random Effect Models for Powerful and Efficient Genome-Wide Association Studies. PLOS Genetics **12**, e1005767.

Miralles DJ, Slafer GA. 2007. PAPER PRESENTED AT INTERNATIONAL WORKSHOP ON INCREASING WHEAT YIELD POTENTIAL, CIMMYT, OBREGON, MEXICO, 20–24 MARCH 2006 Sink limitations to yield in wheat: how could it be reduced? The Journal of Agricultural Science **145**, 139–149.

Mo Y, Vanzetti LS, Hale I, Spagnolo EJ, Guidobaldi F, Al-Oboudi J, Odle N, Pearce S, Helguera M, Dubcovsky J. 2018. Identification and characterization of Rht25, a locus on chromosome arm 6AS affecting wheat plant height, heading time, and spike development. Theoretical and Applied Genetics **131**, 2021–2035.

Nagelmüller S, Kirchgessner N, Yates S, Hiltpold M, Walter A. 2016. Leaf Length Tracker: a novel approach to analyse leaf elongation close to the thermal limit of growth in the field. Journal of Experimental Botany **67**, 1897–1906.

Ochagavía H, Prieto P, Zikhali M, Griffiths S, Slafer GA. 2019. Earliness Per Se by Temperature Interaction on Wheat Development. Scientific Reports **9**, 1–11.

Parent B, Millet EJ, Tardieu F. 2018. The use of thermal time in plant studies has a sound theoretical basis provided that confounding effects are avoided. Journal of Experimental Botany **70**, 2359–2370.

Parent B, Tardieu F. 2012. Temperature responses of developmental processes have not been affected by breeding in different ecological areas for 17 crop species. New Phytologist **194**, 760–774.

Porter JR, Gawith M. 1999. Temperatures and the growth and development of wheat: a review. European Journal of Agronomy **10**, 23–36.

Purcell S, Neale B, Todd-Brown K, *et al.* 2007. PLINK: a tool set for whole-genome association and population-based linkage analyses. American Journal of Human Genetics **81**, 559–575.

R Core Team. 2015. *R: A language and environment for statistical computing*. Vienna, Austria: R Foundation for Statistical Computing.

Rezaei EE, Siebert S, Hüging H, Ewert F. 2018. Climate change effect on wheat phenology depends on cultivar change. Scientific Reports **8**, 4891.

Rodríguez-Álvarez MX, Boer MP, van Eeuwijk FA, Eilers PHC. 2018. Correcting for spatial heterogeneity in plant breeding experiments with P-splines. Spatial Statistics **23**, 52–71.

Roth L, Aasen H, Walter A, Liebisch F. 2018. Extracting leaf area index using viewing geometry effects—A new perspective on high-resolution unmanned aerial system photography. ISPRS Journal of Photogrammetry and Remote Sensing **141**, 161–175.

Sanchez-Bermejo E, Balasubramanian S. 2016. Natural variation involving deletion alleles of FRIGIDA modulate temperature-sensitive flowering responses in Arabidopsis thaliana. Plant, Cell & Environment **39**, 1353–1365.

Schürch C, Kronenberg L, Hund A. 2018. *Wheat developmental stages*.

Sharma N, Ruelens P, D'hauw M, Maggen T, Dochy N, Torfs S, Kaufmann K, Rohde A, Geuten K. 2017. A Flowering Locus C Homolog Is a Vernalization-Regulated Repressor in Brachypodium and Is Cold Regulated in Wheat. Plant Physiology **173**, 1301–1315.

Slafer GA, Calderini DF, Miralles DJ. 1996. Yield components and compensations in wheat: opportunities for further increasing yield potential. In: Reynolds MP, Rajaram S, McNab A, eds. Increasing Yield Potential in Wheat: Breaking the Barriers : Proceedings of a Workshop Held in Ciudad Obregón, Sonora, Mexico. Mexico: CIMMYT, 101–133.

Slafer GA, Kantolic AG, Appendino ML, Tranquilli G, Miralles DJ, Savin R. 2015. Chapter 12 - Genetic and environmental effects on crop development determining adaptation and yield. In: Calderini VOSF, ed. Crop Physiology (Second Edition). San Diego: Academic Press, 285–319.

Slafer GA, Rawson HM. 1994. Sensitivity of Wheat Phasic Development to Major Environmental Factors: a Re-Examination of Some Assumptions Made by Physiologists and Modellers. Functional Plant Biology **21**, 393–426.

Slafer GA, Rawson HM. 1995*a*. Rates and Cardinal Temperatures for Processes of Development in Wheat: Effects of Temperature and Thermal Amplitude. Functional Plant Biology **22**, 913–926.

Slafer GA, Rawson HM. 1995*b*. Intrinsic earliness and basic development rate assessed for their response to temperature in wheat. Euphytica **83**, 175–183.

Slafer GA, Rawson HM. 1995*c*. Photoperiod × temperature interactions in contrasting wheat genotypes: Time to heading and final leaf number. Field Crops Research **44**, 73–83.

Tang Y, Liu X, Wang J, *et al.* 2016. GAPIT Version 2: An Enhanced Integrated Tool for Genomic Association and Prediction. The Plant Genome **9**.

Thines B, Harmon FG. 2010. Ambient temperature response establishes ELF3 as a required component of the core Arabidopsis circadian clock. Proceedings of the National Academy of Sciences **107**, 3257–3262.

Trevaskis B, Hemming MN, Dennis ES, Peacock WJ. 2007. The molecular basis of vernalization-induced flowering in cereals. Trends in Plant Science **12**, 352–357.

VanRaden PM. 2008. Efficient Methods to Compute Genomic Predictions. Journal of Dairy Science **91**, 4414–4423.

Wang S, Wong D, Forrest K, *et al.* 2014. Characterization of polyploid wheat genomic diversity using a high-density 90 000 single nucleotide polymorphism array. Plant Biotechnology Journal **12**, 787–796.

Whitechurch EM, Slafer GA, Miralles DJ. 2007. Variability in the Duration of Stem Elongation in Wheat and Barley Genotypes. Journal of Agronomy and Crop Science **193**, 138–145.

Wigge PA. 2013. Ambient temperature signalling in plants. Current Opinion in Plant Biology **16**, 661–666.

Worland AJ, Sayers EJ, Börner A. 1994. The Genetics and Breeding Potential of Rht12, a Dominant Dwarfing Gene in Wheat. Plant Breeding **113**, 187–196.

Wu J, Kong X, Wan J, *et al.* 2011. Dominant and Pleiotropic Effects of a GAI Gene in Wheat Results from a Lack of Interaction between DELLA and GID1. Plant Physiology **157**, 2120–2130.

Xue W, Xing Y, Weng X, *et al.* 2008. Natural variation inGhd7 is an important regulator of heading date and yield potential in rice. Nature Genetics **40**, 761–767.

Yates S, Mikaberidze A, Krattinger SG, *et al.* 2019. Precision Phenotyping Reveals Novel Loci for Quantitative Resistance to Septoria Tritici Blotch. Plant Phenomics.

Youssefian S, Kirby EJM, Gale MD. 1992. Pleiotropic effects of the GA-insensitive Rht dwarfing genes in wheat. 1. Effects on development of the ear, stem and leaves. Field Crops Research **28**, 179–190.

Zanke CD, Ling J, Plieske J, *et al.* 2014*a*. Genetic architecture of main effect QTL for heading date in European winter wheat. Frontiers in Plant Science **5**.

Zanke C, Ling J, Plieske J, *et al.* 2014*b*. Whole Genome Association Mapping of Plant Height in Winter Wheat (Triticum aestivum L.). PLoS ONE **9**.

Zhang Z, Ersoz E, Lai C-Q, *et al.* 2010. Mixed linear model approach adapted for genome-wide association studies. Nature Genetics **42**, 355–360.

Zheng X, Levine D, Shen J, Gogarten SM, Laurie C, Weir BS. 2012. A high-performance computing toolset for relatedness and principal component analysis of SNP data. Bioinformatics **28**, 3326–3328.

Zikhali M, Griffiths S. 2015. The Effect of Earliness per se (Eps) Genes on Flowering Time in Bread Wheat. Advances in Wheat Genetics: From Genome to Field. Springer, Tokyo, 339–345.

Zikhali M, Wingen LU, Griffiths S. 2016. Delimitation of the Earliness per se D1 (Eps-D1) flowering gene to a subtelomeric chromosomal deletion in bread wheat (Triticum aestivum). Journal of Experimental Botany **67**, 287–299.

Tables

Table 1: Variance components and heritabilities for all investigated traits.

Trait	var. comp.	estimate	std.error	z.ratio	% tot. var.	Heritability
$int_{SER\sim T}$	Gen_ID	7.024E-07	7.219E-08	9.730	49.01	0.77
	Gen_ID:Year	5.224E-07	3.491E-08	14.963	36.45	
	units!R	2.084E-07	8.920E-09	23.365	14.54	
$slp_{SER\sim T}$	Gen_ID	7.348E-08	7.184E-09	10.229	55.00	0.81
	Gen_ID:Year	4.516E-08	2.925E-09	15.440	33.80	
	units!R	1.495E-08	6.396E-10	23.372	11.19	
FH	Gen_ID	1.226E-02	9.798E-04	12.511	92.24	0.98
	Gen_ID:Year	5.890E-04	4.568E-05	12.893	4.43	
	units!R	4.417E-04	1.890E-05	23.371	3.32	
GDD_{15}	Gen_ID	1.226E+03	1.171E+02	10.471	56.64	0.82
	Gen_ID:Year	6.241E+02	4.370E+01	14.283	28.84	
	units!R	3.144E+02	1.345E+01	23.365	14.53	
GDD_{95}	Gen_ID	1.190E+03	1.120E+02	10.624	56.84	0.84
	Gen_ID:Year	4.953E+02	3.958E+01	12.515	23.66	
	units!R	4.081E+02	1.747E+01	23.365	19.50	
$time_{SE}$	Gen_ID	5.844E+00	8.095E-01	7.219	27.84	0.59
	Gen_ID:Year	9.481E+00	6.911E-01	13.717	45.16	
	units!R	5.668E+00	2.425E-01	23.370	27.00	
GDD_{SE}	Gen_ID	5.665E+02	8.544E+01	6.631	24.14	0.54
	Gen_ID:Year	1.067E+03	8.007E+01	13.326	45.46	
	units!R	7.134E+02	3.052E+01	23.375	30.40	
$heading_{GDD}$	Gen_ID	1.742E+03	1.481E+02	11.764	80.24	0.92
	units!R	4.290E+02	2.380E+01	18.028	19.76	

Table 2: Type-II analysis of variance table for the linear model[1] used to predict final canopy height based on temperature response ($slp_{SER\sim T}$) vigour ($int_{SER\sim T}$) and stem elongation duration (GDD_{SE}). *Rht-B1*, *Rht-D1* and *Ppd-D1* alleles and all two-way interactions[2] were included to test for possible confounding of temperature response with final height or photoperiod. The model was applied on the 3-Year BLUES of all genotypes with available allelic data of the respective genes (n = 301)

predictor	Sum Sq	Df	F value	Pr(>F)	
$slp_{SER\sim T}$	7.63E-01	1	2.43E+03	5.08E-140	***
$int_{SER\sim T}$	5.91E-01	1	1.88E+03	2.57E-126	***
GDD_{SE}	1.29E-01	1	4.12E+02	5.74E-57	***
Rht-B1	3.16E-03	1	1.01E+01	1.69E-03	**
Rht-D1	3.53E-03	1	1.12E+01	9.13E-04	***
Ppd-D1	1.48E-06	1	4.71E-03	9.45E-01	
$slp_{SER\sim T}$: $int_{SER\sim T}$	2.56E-04	1	8.16E-01	3.67E-01	
$slp_{SER\sim T}$:GDD_{SE}	2.31E-05	1	7.36E-02	7.86E-01	
$int_{SER\sim T}$:GDD_{SE}	9.76E-06	1	3.11E-02	8.60E-01	
Rht-B1:*Ppd-D1*	8.94E-04	1	2.85E+00	9.26E-02	.
Rht-D1:*Ppd-D1*	1.42E-03	1	4.51E+00	3.45E-02	*
$slp_{SER\sim T}$:*Rht-B1*	4.01E-06	1	1.28E-02	9.10E-01	
$slp_{SER\sim T}$:*Rht-D1*	1.43E-06	1	4.56E-03	9.46E-01	
$slp_{SER\sim T}$:*Ppd-D1*	5.53E-04	1	1.76E+00	1.85E-01	
$int_{SER\sim T}$:*Rht-B1*	9.01E-04	1	2.87E+00	9.13E-02	.
$int_{SER\sim T}$:*Rht-D1*	7.02E-04	1	2.23E+00	1.36E-01	
$int_{SER\sim T}$:*Ppd-D1*	7.70E-04	1	2.45E+00	1.19E-01	
GDD_{SE}:*Rht-B1*	1.71E-05	1	5.46E-02	8.15E-01	
GDD_{SE}:*Rht-D1*	7.56E-04	1	2.41E+00	1.22E-01	
GDD_{SE}:*Ppd-D1*	4.48E-05	1	1.43E-01	7.06E-01	
Residuals	8.79E-02	280			

[1]see eq. 6

[2]The interaction effect of *Rht-B1* and *Rht-D1* was dropped due to singularity.

Table 3: Marker-trait associations for $slp_{SER\sim T}$, $int_{SER\sim T}$, GDD_{15}, GDD_{95} $heading_{GDD}$ and FH, including *P*-value, minor allele frequency and allelic effect estimate

Trait	SNP	Chr	Position	*P*-value	maf	effect
$slp_{SER\sim T}$	wsnp_Ex_c1597_3045682	1B	688'283'256	1.76E-06	0.19	-6.05E-05
	CAP7_c10839_300	4B	533'724'424	4.17E-06	0.24	-5.07E-05
	IAAV7104	5D	553'678'522	9.67E-06	0.13	-6.02E-05
$int_{SER\sim T}$	RAC875_s109189_188	2B	248'149'774	5.08E-07	0.42	1.73E-04
	Ku_c63300_1309	4B	21'556'672	2.73E-06	0.10	-2.99E-04
	Kukri_rep_c68594_530	4D	12'773'259	7.47E-09	0.40	-2.30E-04
	Kukri_c6477_696	5D	423'502'809	3.89E-07	0.21	-2.03E-04
GDD_{15}	wsnp_Ex_c12447_19847242	1D	416'456'386	1.91E-06	0.46	6.89E+00
	Tdurum_contig47508_250	2A	754'339'235	1.31E-06	0.21	9.41E+00
	Kukri_c55381_67	3A	648'868'234	1.38E-06	0.17	-1.00E+01
	Excalibur_c74858_243	5B	13'190'663	2.50E-08	0.47	-7.88E+00
GDD_{95}	Excalibur_c49597_579	5A	521'934'666	1.19E-06	0.42	-6.58E+00
	Excalibur_c74858_243	5B	13'190'663	6.15E-07	0.47	-6.14E+00
	Tdurum_contig44115_561	5B	669'897'388	2.31E-07	0.13	-1.02E+01
	RAC875_c38693_319	7B	740'056'880	2.87E-06	0.20	7.51E+00
$heading_{GDD}$	RAC875_c12766_461	2B	47'430'682	2.10E-07	0.39	-7.77E+00
	Kukri_rep_c106620_208	3A	714'300'397	1.55E-07	0.08	1.47E+01
	BS00022611_51	3B	659'787'924	2.83E-06	0.12	8.75E+00
	IAAV7221	4B	2'036'611	9.96E-07	0.07	-1.29E+01
	BS00000365_51	5A	538'000'573	5.19E-07	0.44	-7.65E+00
	IACX2540	5A	619'684'943	4.73E-08	0.35	9.39E+00
	Excalibur_c74858_243	5B	13'190'663	1.16E-08	0.47	-8.67E+00
	Excalibur_c46904_84	7D	5'198'912	3.55E-06	0.13	-9.46E+00
FH	Excalibur_c85499_232	1A	582'219'427	2.23E-08	0.11	2.52E-02
	wsnp_Ku_c11665_18999583	2B	139'070'721	9.07E-07	0.13	2.08E-02
	Kukri_c49280_230	3A	20'134'735	1.63E-07	0.08	2.90E-02
	Tdurum_contig64772_417	4B	26'491'482	4.18E-09	0.07	3.56E-02
	RAC875_rep_c105718_585	4D	25'989'162	2.20E-12	0.38	-2.56E-02
	BS00036421_51	4D	32'347'318	3.96E-07	0.37	-1.58E-02
	RAC875_c8231_1578	5A	613'588'253	1.52E-06	0.43	1.44E-02
	wsnp_Ku_rep_c71232_70948744	5A	679'663'586	7.93E-10	0.47	-2.21E-02
	BS00109560_51	5B	556'182'591	6.91E-07	0.46	-1.56E-02
	BS00022120_51	6A	396'301'470	1.68E-07	0.24	-2.01E-02

Table 4: Selected putative candidate genes for temperature response ($slp_{SER\sim T}$) from the IWGSC reference genome annotation

Chr	SNP [Position]	r.start	r.end	Gene	description	distance
chr1B	wsnp_Ex_c1597_3045682 [688'283'256]	688'282'509	688'286'431	TraesCS1B01G480600	winged-helix DNA-binding transcription factor family protein	747
		688'352'414	688'354'696	TraesCS1B01G480700	HMG-Y-related protein A	-69'158
		687'710'716	687'719'885	TraesCS1B01G480100	Argonaute	572'540
		687'128'952	687'135'442	TraesCS1B01G479200	Zinc finger protein CONSTANS	1'154'304
		687'078'233	687'084'562	TraesCS1B01G479000	Zinc finger protein CONSTANS	1'205'023
		686'928'468	686'931'886	TraesCS1B01G478700	Zinc finger protein CONSTANS	1'354'788
		686'749'516	686'755'405	TraesCS1B01G478100	WD-repeat protein, putative	1'533'740
		685'645'287	685'649'392	TraesCS1B01G477400	Early flowering 3	2'637'969
chr4B	CAP7_c10839_300 [533'724'424]	537'474'959	537'479'867	TraesCS4B01G266000	Protein FRIGIDA	-3'750'535
		541'363'317	541'365'139	TraesCS4B01G267700	Protein upstream of flc	-7'638'893
		542'582'729	542'583'265	TraesCS4B01G268300	MADS transcription factor	-8'858'305
chr5D	IAAV7104 [553'678'522]	554'357'761	554'360'305	TraesCS5D01G544800	FRIGIDA-like protein, putative	-679'239
		554'467'487	554'472'596	TraesCS5D01G545100	Transducin/WD-like repeat-protein	-788'965
		556'226'523	556'234'480	TraesCS5D01G548800	Transducin/WD-like repeat-protein	-2'548'001

Table 5: Selected putative candiate genes for vigour ($int_{SER\sim T}$) of temperature response from the IWGSC reference genome annotation

Chr	SNP [Position]	r.start	r.end	Gene	description	distance
chr2B	RAC875_s109189_188 [248’149’774]	243'569'388	243'571'100	TraesCS2B01G239400	GRAS transcription factor	4'580'386
chr4B	Ku_c63300_1309 [21’556’672]	21'187'173	21'192'244	TraesCS4B01G028500	Tesmin/TSO1-like CXC domain-containing protein	369'499
		20'005'649	20'008'978	TraesCS4B01G026600	Argonaute family protein	1'551'023
		19'740'974	19'744'058	TraesCS4B01G026200	WD40 repeat-like protein	1'815'698
		23'404'428	23'408'188	TraesCS4B01G031300	BHLH family protein, putative, expressed	-1'847'756
		23'818'506	23'822'972	TraesCS4B01G032000	Protein UPSTREAM OF FLC	-2'261'834
		18'162'363	18'165'744	TraesCS4B01G025500	Homeobox protein BEL1 like	3'394'309
		18'091'908	18'093'975	TraesCS4B01G025400	BEL1-like homeodomain protein	3'464'764
		17'229'197	17'236'874	TraesCS4B01G024000	Argonaute protein	4'327'475
		17'017'132	17'019'148	TraesCS4B01G023300	AGAMOUS-like MADS-box transcription factor	4'539'540
		26'335'682	26'336'740	TraesCS4B01G036600	BRI1 suppressor 1 (BSU1)-like 3	-4'779'010
		26'824'399	26'827'490	TraesCS4B01G037200	WD-repeat protein, putative	-5'267'727
		15'427'017	15'431'870	TraesCS4B01G021500	basic helix-loop-helix (bHLH) DNA-binding superfamily protein	6'129'655
		15'259'656	15'263'139	TraesCS4B01G021200	basic helix-loop-helix (bHLH) DNA-binding superfamily protein	6'297'016
		15'146'117	15'150'854	TraesCS4B01G021100	Basic helix loop helix (BHLH) DNA-binding family protein	6'410'555
		14'710'395	14'711'057	TraesCS4B01G020800	Protein FAR1-RELATED SEQUENCE 5	6'846'277
		28'413'432	28'414'112	TraesCS4B01G041000	sensitive to freezing 6	-6'856'760
		29'673'211	29'674'674	TraesCS4B01G042500	Fantastic four-like protein	-8'116'539
chr4D	Kukri_rep_c68594_530 [12’773’259]	12'700'119	12'703'878	TraesCS4D01G028900	BHLH family protein, putative, expressed	73'140
		13'096'296	13'096'966	TraesCS4D01G029600	CLAVATA3/ESR (CLE)-related protein 25	-323'037
		13'196'859	13'200'535	TraesCS4D01G029700	Protein UPSTREAM OF FLC	-423'600
		11'364'404	11'369'466	TraesCS4D01G026100	Tesmin/TSO1-like CXC domain-containing protein	1'408'855
		10'746'363	10'750'251	TraesCS4D01G024300	Argonaute protein	2'026'896
		10'684'336	10'690'389	TraesCS4D01G024100	Argonaute family protein	2'088'923
		10'254'979	10'257'683	TraesCS4D01G023600	WD40 repeat-like protein	2'518'280
		15'768'990	15'772'059	TraesCS4D01G034500	WD-repeat protein, putative	-2'995'731
		9'495'616	9'501'619	TraesCS4D01G022600	Homeobox protein BEL1 like	3'277'643
		9'443'778	9'445'575	TraesCS4D01G022500	BEL1-like homeodomain protein 1	3'329'481
		9'069'403	9'071'423	TraesCS4D01G021100	MADS-box transcription factor	3'703'856
		16'584'271	16'584'948	TraesCS4D01G038400	sensitive to freezing 6	-3'811'012

		8'777'205	8'779'670	TraesCS4D01G020300	Growth-regulating factor	3'996'054
		8'149'046	8'151'425	TraesCS4D01G019200	basic helix-loop-helix (bHLH) DNA-binding superfamily protein	4'624'213
		8'135'666	8'137'454	TraesCS4D01G019100	basic helix-loop-helix (bHLH) DNA-binding superfamily protein	4'637'593
		8'010'719	8'012'446	TraesCS4D01G018800	basic helix-loop-helix (bHLH) DNA-binding superfamily protein	4'762'540
		7'992'104	7'995'445	TraesCS4D01G018700	basic helix-loop-helix (bHLH) DNA-binding superfamily protein	4'781'155
		17'765'786	17'767'021	TraesCS4D01G039900	Fantastic four-like protein	-4'992'527
		18'781'062	18'782'933	TraesCS4D01G040400	GAI-like protein 1 **(*Rht-D1*)**	-6'007'803
		6'703'246	6'703'509	TraesCS4D01G015200	SAUR-like auxin-responsive protein family	6'070'013
		6'699'039	6'699'458	TraesCS4D01G015100	SAUR-like auxin-responsive protein family	6'074'220
		6'682'318	6'682'602	TraesCS4D01G015000	SAUR-like auxin-responsive protein family	6'090'941
		6'663'820	6'664'131	TraesCS4D01G014900	SAUR-like auxin-responsive protein family	6'109'439
		6'461'624	6'462'688	TraesCS4D01G013800	BRI1 suppressor 1 (BSU1)-like 3	6'311'635
		19'169'377	19'171'147	TraesCS4D01G040600	Protein FAR1-RELATED SEQUENCE 5	-6'396'118
		6'017'847	6'023'948	TraesCS4D01G012800	Protein FAR1-RELATED SEQUENCE 5	6'755'412
		4'128'933	4'133'919	TraesCS4D01G008400	WD-repeat protein, putative	8'644'326
		21'775'252	21'776'785	TraesCS4D01G046200	CONSTANS-like zinc finger protein	-9'001'993
chr5D	Kukri_c6477_696 [423’502’809]	423'858'756	423'860'766	TraesCS5D01G334100	Armadillo repeat only	-355'947
		421'503'514	421'504'332	TraesCS5D01G329500	HVA22-like protein	1'999'295
		426'296'827	426'301'957	TraesCS5D01G337800	WD-repeat protein, putative	-2'794'018
		429'289'426	429'292'023	TraesCS5D01G341000	CONSTANS-like zinc finger protein	-5'786'617
		416'787'868	416'788'986	TraesCS5D01G325300	Protein Mei2	6'714'941
		416'625'946	416'628'639	TraesCS5D01G325200	Protein Mei2	6'876'863
		415'622'032	415'622'615	TraesCS5D01G323500	Auxin-responsive protein	7'880'777

Table 6: Type II analysis of variance for the prediction of final height using QTL and *Rht-B1*, *Rht-D1* and *Ppd-D1* alleles. SNP alleles of the QTL for temperature response ($slp_{SER\sim T}$), vigour ($int_{SER\sim T}$), start (GDD_{15}) and end (GDD_{95}) of stem elongation as well as *Rht-B1*, *Rht-D1* and *Ppd-D1* alleles were used as predictors in a linear model (FH = ∑ QTL $slp_{SER\sim T}$ + ∑ QTL $int_{SER\sim T}$ + ∑ QTL GDD_{15} + ∑ QTL GDD_{95} + *Rht-B1* + *Rht-D1* + *Ppd-D1*) without interaction effects (see Fig. 6B). The model was applied to the 3-year BLUES of all genotypes with available genotypic data (n = 300) on all predictors.

Predictor [trait.QTL.chromosome]	SNP	Sum Sq	Df	F value	Pr(>F)	
$slp_{SER\sim T}$.1.1B	wsnp_Ex_c1597_3045682	4.20E-03	1	1.08E+00	2.99E-01	
$slp_{SER\sim T}$.2.4B	CAP7_c10839_300	7.97E-03	1	2.05E+00	1.53E-01	
$slp_{SER\sim T}$.3.5D	IAAV7104	2.81E-02	1	7.23E+00	7.58E-03	**
$int_{SER\sim T}$.1.2B	RAC875_s109189_188	1.72E-03	1	4.42E-01	5.07E-01	
$int_{SER\sim T}$.2.4B	Ku_c63300_1309	1.64E-02	1	4.23E+00	4.07E-02	*
$int_{SER\sim T}$.3.4D	Kukri_rep_c68594_530	7.47E-03	1	1.93E+00	1.66E-01	
$int_{SER\sim T}$.4.5D	Kukri_c6477_696	6.06E-03	1	1.56E+00	2.13E-01	
GDD_{15}.1.1D	wsnp_Ex_c12447_19847242	1.41E-02	1	3.64E+00	5.74E-02	.
GDD_{15}.2.2A	Tdurum_contig47508_250	4.97E-02	1	1.28E+01	4.07E-04	***
GDD_{15}.3.3A	Kukri_c55381_67	1.91E-02	1	4.91E+00	2.75E-02	*
GDD_{15}.4|GDD_{95}.2|heading.7.5B	Excalibur_c74858_243	7.64E-08	1	1.97E-05	9.96E-01	
GDD_{95}.1.5A	Excalibur_c49597_579	4.04E-02	1	1.04E+01	1.40E-03	**
GDD_{95}.3.5B	Tdurum_contig44115_561	1.03E-03	1	2.65E-01	6.07E-01	
GDD_{95}.4.7B	RAC875_c38693_319	4.28E-03	1	1.10E+00	2.95E-01	
Rht-B1		3.32E-01	1	8.55E+01	6.02E-18	***
Rht-D1		6.71E-01	1	1.73E+02	3.79E-31	***
Ppd-D1		5.87E-02	1	1.51E+01	1.26E-04	***
Residuals		1.09E+00	282			

Figures with figure legends

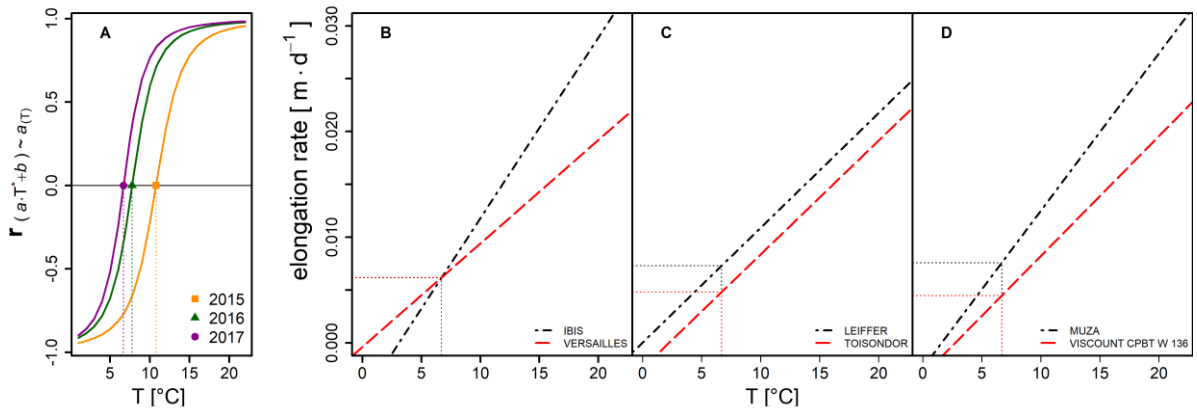

Fig. 1: Illustration and interpretation for the parameters of the applied temperature response model (eq. 2). A: Distribution of Pearson correlation coefficients between intercept and slope of the linear model for individual years, depending on the temperature, at which the intercept is calculated. Dotted vertical lines indicate the critical temperature (T_{crit}) for individual years used to calculate the intercept. **B-D**: Illustration of the relation between intercept and slope on contrasting genotypes (dashed and dash-dotted lines). **B**: same vigour but different in temperature response. **C** both have the same T-response but differ in vigour. **D** Genotypes differ in vigour as well as in T-response. Horizontal and vertical dotted lines indicate vigour and T_{crit} respectively. The two contrasting genotypes per example (B-D) were selected from the 2017 data based on their vales for slope and intercept.

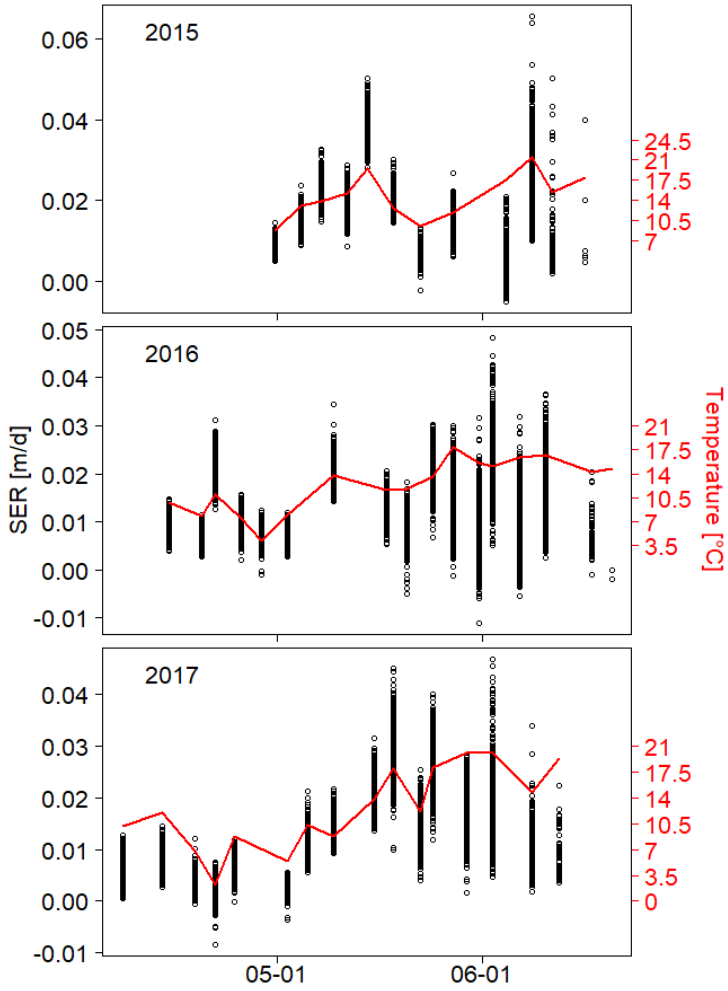

Fig. 2: **Relationship between stem elongation rate (SER) and temperature.** Plot based SER raw data (n > 700/a) of > 330 genotypes (black dots) as well as temperature (solid red line) is plotted against calendar time for the years 2015-2017

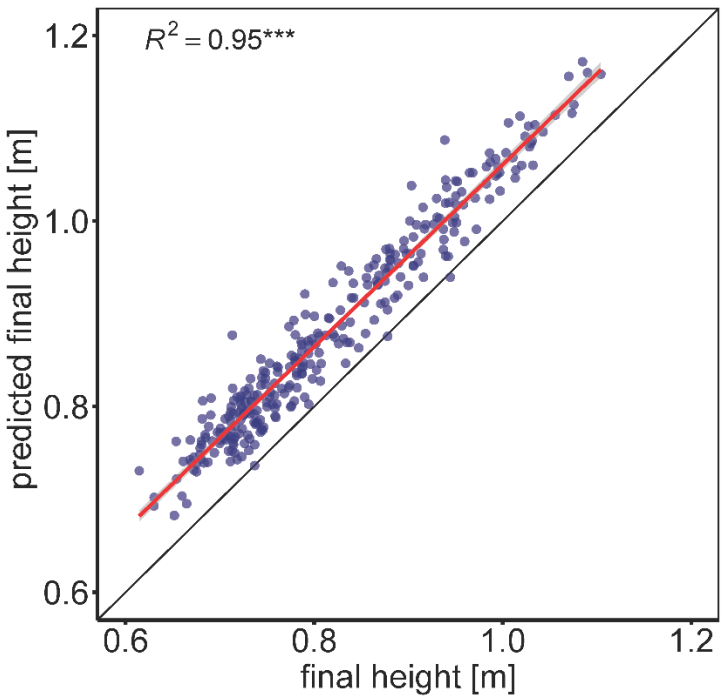

Fig. 3: Prediction of final height based on temperature response ($slp_{SER\sim T}$) vigour ($int_{SER\sim T}$) and stem elongation duration (GDD_{SE}). *Rht-B1*, *Rht-D1* and *Ppd-D1* alleles and all two-way interactions were included to test for possible confounding of temperature response with final height or photoperiod (see eq. 6 and Table 2). The model was applied on the 3-Year BLUES of all genotypes with available allelic data of the respective genes (n = 301).

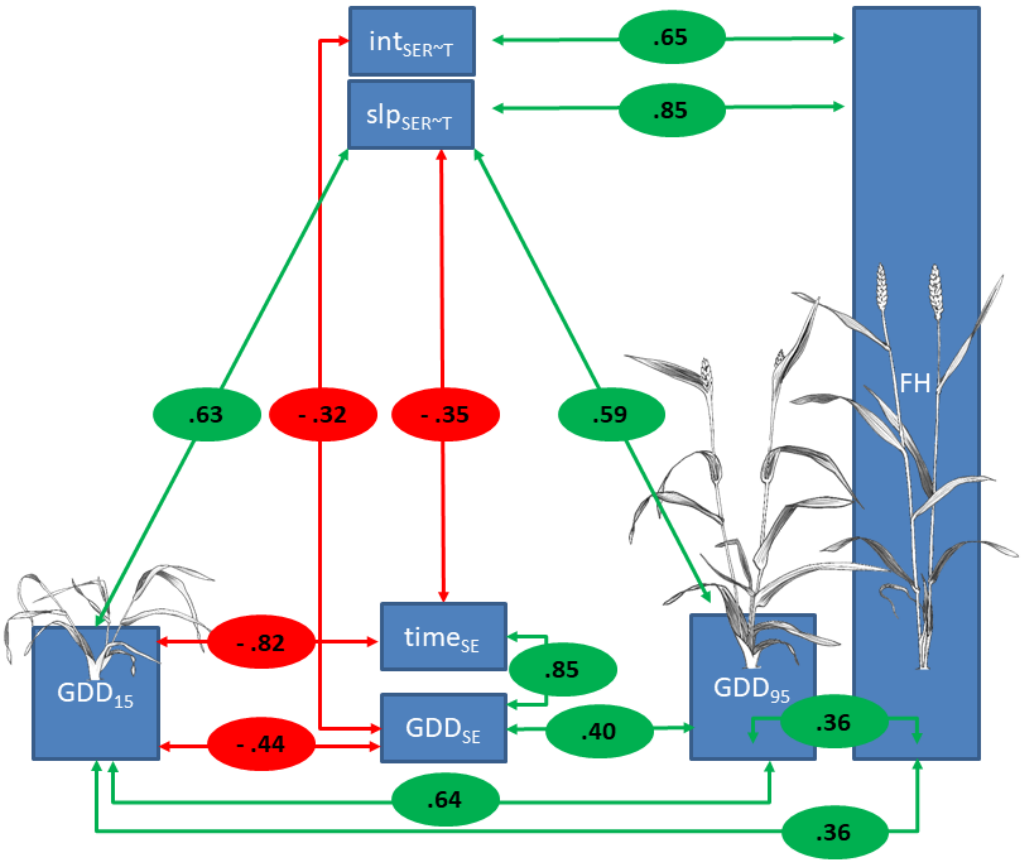

Fig 4. Key correlations among investigated traits. Pearson correlation coefficients between respective traits are given in red and green circles, where red denotes a negative correlation and green denotes a positive correlation. Weak correlations (r < 0.3) are shown in the complete correlation matrix Fig. S3. Illustrations of GDD_{15}, GDD_{95} and FH were taken from Schürch *et al.* (2018).

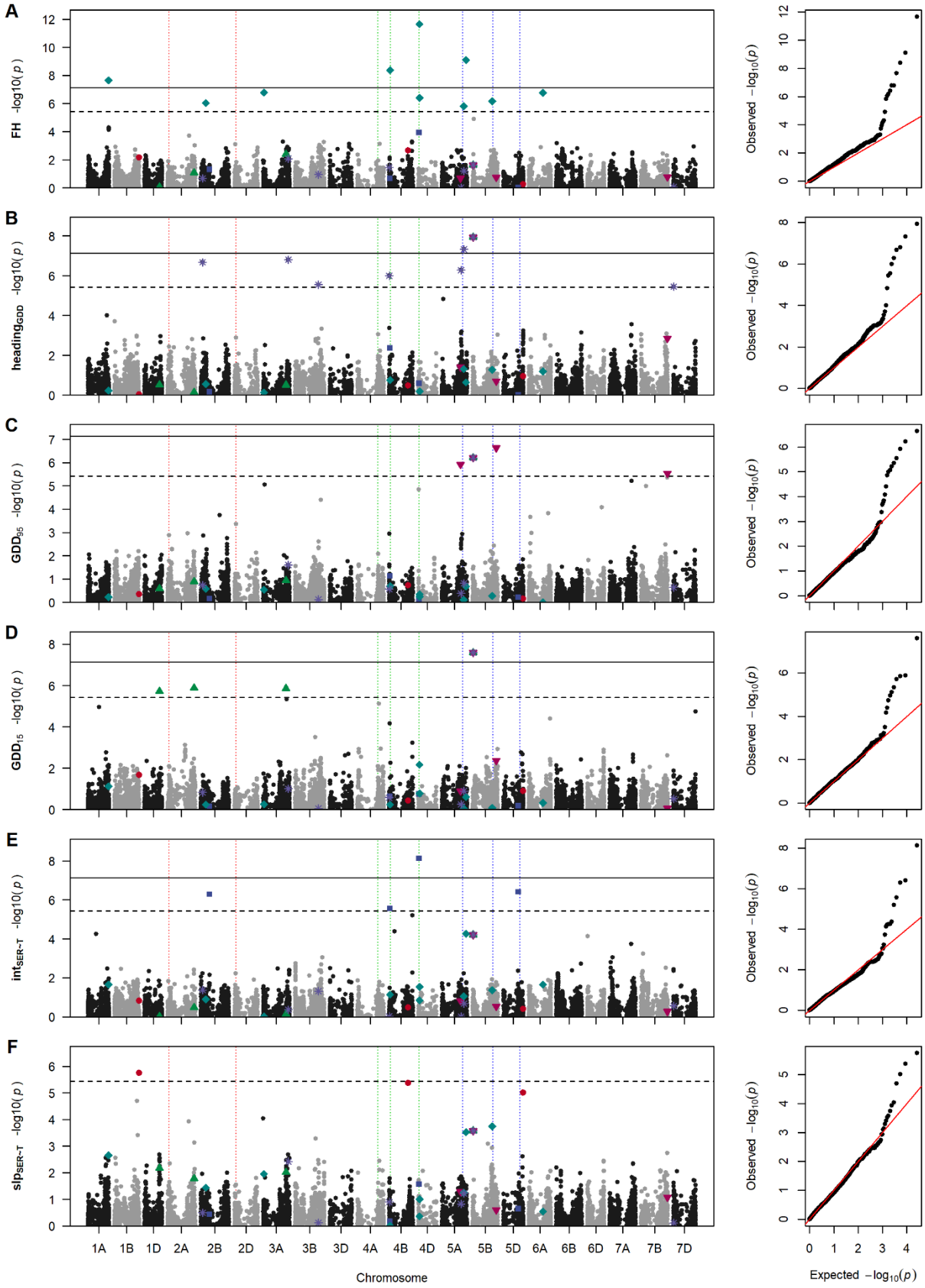

Fig. 5 Manhattan plots and quantile-quantile plots depicting the GWAS results using FarmCPU for final height (FH, A), growing degree days until heading (heading$_{GDD}$, B); end (GDD$_{95}$, C) and start (GDD$_{15}$, D) of stem elongation; vigour-related intercept (int$_{SER\sim T}$, E) and

temperature-related slope ($slp_{SER\sim T}$, F) of stem elongation in response to temperature. Horizontal lines mark the Bonferroni corrected significance threshold for $P < 0.05$ (dashed line) and $P < 0.001$ (solid line). Vertical dotted lines mark the positions of *Ppd-1* on chromosomes 2A and 2D (red), *Rht-1* on chromosomes 4A-4D (green) and *Vrn-1* on chromosomes 5A-5D. Significant marker trait associations for $slp_{SER\sim T}$ (red dots), $int_{SER\sim T}$ (blue squares), GDD_{15} (green up-facing triangles), GDD_{95} (magenta down-facing triangles), heading (violet asterisks) and FH (turquois diamonds) are highlighted in all manhattan plots.

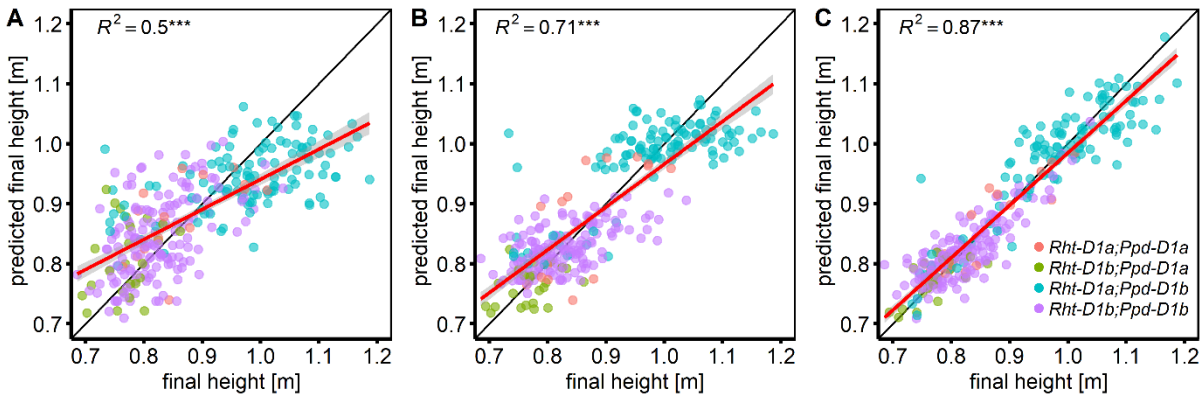

Fig6: Prediction of final height based on QTL and *Rht-B1*, *Rht-D1* and *Ppd-D1* alleles. A: The SNP alleles of significantly associated QTL for temperature response ($slp_{SER\sim T}$), vigour ($int_{SER\sim T}$), start (GDD_{15}) and end (GDD_{95}) of stem elongation were used in a linear model without considering interaction effects. **B:** *Rht-B1*, *Rht-D1* and *Ppd-D1* alleles were added to the model used in A. **C:** All two-way interaction effects among SNP alleles and *Rht-B1*, *Rht-D1* and *Ppd-D1* alleles were included in the model. The models were applied to the 3-year BLUES of all genotypes with available genotypic data (n = 300) on all predictors. Colours indicate the allelic status regarding *Rht-D1* and *Ppd-D1* of the respective genotypes as depicted in panel C.